

## CHAPTER 5

### STATISTICAL SIGNIFICANCE TEST OF INTRINSIC MODE FUNCTIONS

Zhaohua Wu and Norden E. Huang

One of the preliminary tasks when analyzing a dataset is to determine whether it or its components contain useful information. The task is essentially a binary hypothesis testing problem in which a null hypothesis of pure noise is often pre-proposed. To test against the null hypothesis, the characteristics of noise need to be understood first, and often, these characteristics pertain to the analysis method used.

In this paper, the characteristics of Gaussian white noise are studied by using the empirical mode decomposition (EMD) method. Statistical testing methods for Gaussian white noise for the intrinsic mode functions (IMFs) are designed based on the characteristics of Gaussian white noise by using EMD. These methods are applied to well-studied geophysical datasets to demonstrate the method's validity and effectiveness.

#### 5.1. Introduction

The word “noise” can possibly be traced back to the Latin word “nausea,” “seasickness, feeling of sickness.” In the scientific community, “noise” refers to a disturbance, especially a random and persistent disturbance that obscures or reduces the clarity of a signal. The causes of noise are numerous. In radar, noise is often caused by ambient radiation and the receiver's electronics. In a digital communication system, the signal is usually distorted due to limited channel bandwidth and is corrupted by additive channel noise. In nature, noise can be generated by local and intermittent instabilities, irresolvable sub-grid phenomena, some concurrent phenomena in the environment where investigations are being conducted, and by the sensors and recording systems. As a result, when we are dealing with data, we are inevitably dealing with an amalgamation of signal and noise,

$$x(t) = s(t) + n(t), \quad (5.1)$$

where  $x(t)$  denotes the data, and  $s(t)$  and  $n(t)$  are the signal and noise, respectively.

The detection of the information content of a noisy dataset is fundamental to decision making and information extraction. Usually, the extraction of information requires a knowledge of the characteristics of both the signal and the noise. When the processes that generate the dataset are linear, and the noise in the data has

distinct characteristics from those of the true signal, effective filters can be designed based on the characteristics of the signal and the noise to separate a dataset's signal from the noise. However, such cases are relatively rare since knowledge of the signal in a noisy dataset is limited prior to the analysis of the data. The problem can be more complicated if the signal is nonlinear and nonstationary, and the data is of limited size. In such cases, a short piece of pure noise data may behave like a signal, and therefore, all the possible behaviors of a short piece of noise should be considered. Under such circumstances, a less ambitious goal is often set to decide whether a noisy dataset has any signals. The latter is often a binary hypothesis testing problem associated with a null hypothesis that assumes the dataset contains only noise. Under such a hypothesis, the characteristics of noise can be used as a reference for discriminating the data (or their components) from pure noise without having any pre-knowledge of the signal. Furthermore, knowing the characteristics of the noise is an essential first step before one can attach any significance to the signal eventually extracted from the data. The characteristics of noise are usually related closely to the analysis methods used to examine the noise. For example, white noise in the temporal domain is characterized by the independence among any data points with a zero autocorrelation, whereas in the Fourier frequency domain by a flat Fourier spectra.

Many time-series-analysis methods are currently available for use. When the processes generating the data are linear, and the noises have distinct time or frequency scales different from those of the true signal, these analysis methods may have some capability of distinguishing the data from noise. However, most of these methods suffer more or less from various drawbacks even in linear and stationary cases. For example, even if the real signal and the noises have distinct fundamental frequencies, their harmonics can still mix with the noise during a Fourier spectrum analysis. This mixing of the harmonics with noise will make the Fourier spectrum analysis an ineffective noise-discriminating method. The problem could be even worse when the time series to be analyzed is both nonlinear and non-stationary. Therefore, more effective methods, as well as an understanding of the characteristics of noise pertaining to these methods, are needed so that the signal content of real data can be estimated.

In recent years, a new method, entitled empirical mode decomposition (EMD), has been developed (Huang et al. 1998; Huang et al. 1999; Huang et al. 2003) and has been applied to various fields of scientific research and industry. In this book, the method is introduced and many new applications are illustrated. EMD is an adaptive method to decompose any time series into a set of intrinsic mode function (IMF) components, which become the basis for representing the data. Because the basis is adaptive and locally determined, it usually offers a more physically meaningful representation of the underlying processes. Due to the adaptive nature of the basis, harmonics are not needed; therefore, EMD is ideally suited for analyzing data generated by nonlinear, non-stationary processes.

In this chapter, we will examine the characteristics of Gaussian white noise by using EMD and then design statistical test methods to distinguish the IMFs of real data from those of Gaussian white noise. The characteristics of uniform white noise revealed by using EMD have already been reported (Wu and Huang 2004). Some characteristics of white noise described in Wu and Huang and in this chapter can also be found in a study by Flandrin et al. (2004) and a chapter by Flandrin et al. in this book. We will show that if we know the characteristics of the noise, we can offer some measure of the information content of signals buried under data with an unknown noise level.

In this chapter, we will demonstrate that Gaussian white noise has almost identical characteristics to those of uniform white noise, which we have already reported (Wu and Huang 2004): (1) the EMD is an effective dyadic filter capable of separating white noise into IMFs having mean periods exactly twice the value of the previous one; (2) the IMFs are all normally distributed; and (3) the Fourier spectra of the IMF components are identical in shape and cover the same area on a semi-logarithmic period scale. These results are useful for determining the relationship between the product of the mean energy density of an IMF and its corresponding mean period and also the spread function of the energy density. The characteristics and the derived relationships are verified by using the Monte-Carlo method, which analyzes a large synthetically generated Gaussian white noise dataset. These quantities also provide the necessary information for us to design a statistical significance test method by using the bounds for the energy density spread function of the IMFs of Gaussian white noise. Some well-known climate time series are used to illustrate the effectiveness of the methodology of assigning statistical significance.

The chapter is arranged as follows: Section 5.2 will present the numerical experiment and the empirical relationship between the energy density and the mean period. Section 5.3 will focus on the empirical result of normally distributed IMF components, and the energy spread function derived. Section 5.4 will discuss the statistical significance test method and illustrate its validity by applying the method to some well-known climate time series and to the series defined using climate system model outputs. A discussion and some conclusions will be presented in section 5.5.

## 5.2. Characteristics of Gaussian white noise in EMD

This section is on the statistical characteristics of the IMF components of the Gaussian white noise. These characteristics are derived by numerically studying a lengthy Gaussian white noise of  $2^{20}$  data points generated by using a method described by Press et al. (1992). We are forced to use numerical methods since EMD is an algorithm, and the IMFs have no analytical expression. The empirical results presented below are not sensitive to the random number generators.

**Table 5.1:** The mean periods of IMFs. Each column corresponds to an IMF. The second row is the number of maxima; the third row is the mean period calculated from the number of maxima; and the fourth row is the Fourier spectrum weighted mean period [see (5.8)].

IMFs	1	2	3	4	5
number of maxima	365358	173012	86247	43152	21701
Mean Period (counting extrema)	2.870	6.061	12.16	24.30	50.65
Mean Period (Spec.-weighted)	3.467	5.405	9.841	18.61	35.45

IMFs	6	7	8	9
number of maxima	10843	5429	2717	1345
Mean Period (counting extrema)	96.71	193.1	385.9	779.6
Mean Period (Spec.-weighted)	67.81	133.7	259.4	492.4

### 5.2.1. Numerical experiment

The Gaussian white noise data generated are decomposed into IMFs by using the EMD method. An IMF is any function having symmetric envelopes defined by the local maxima and minima separately, and also having the same number of zero-crossing and extrema. Practically, an IMF is extracted through a sifting process which stops when a certain criterion is satisfied. In this study, a Cauchy-type stoppage criterion modified from that in Huang et al. (1998) is used; i.e.,

$$SC = \frac{\sum_{i=1}^N [h_{n,k+1}(i) - h_{n,k}(i)]^2}{\sum_{i=1}^N h_{n,k}^2(i)} < 2 \times 10^{-4}, \quad (5.2)$$

where  $N$  is the length of data being decomposed and  $h_{n,k}$  is the  $k$ th sifting result for  $n$ th IMF. This modification essentially eliminates the unstable jump of the value of the traditional Cauchy-type stoppage criterion defined in Huang et al. (1998) in the sifting process and is consistent with the stoppage criterion of the repetitiveness of the number of extrema described in Huang et al. (2003). In the experiment, the number of the iteration of the sifting process for each IMF is between seven and ten.

### 5.2.2. Mean periods of IMFs

Based on the definition of an IMF, we can determine the mean period of an IMF by counting the number of local maxima of the function. The results of the mean

periods are listed in Table 5.1. In this table, the second row is the total number of local maxima, the peaks of each IMF in  $2^{20}$  data points. The third row is the extrema-counting mean period measured in terms of the number of data points ( $2^{20}$  divided by total number of maxima of an IMF). The fourth row is the spectrum weighed mean period of an IMF, as defined by (5.8) later. (The spectrum-weighted mean period of an IMF is smaller than the corresponding extrema-counting mean period defined. We will further discuss the issue in section 5.3.) The mean period of the  $n$ th IMF of Gaussian white noise based on extrema counting is slightly larger than that of the  $n$ th IMF of uniformly distributed white noise, which we have already reported on (Wu and Huang 2004). However, the mean period doubling property remains since EMD serves as a dyadic filter, consistent with the results obtained by Flandrin et al. (2004).

### 5.2.3. The Fourier spectra of IMFs

Another characteristic that we are interested in is the detailed distribution of the energy density of an IMF in terms of the Fourier spectrum as a function of its period (the inverse of frequency). The derivation here follows what is described in Wu and Huang (2004), which provides more details. Since the IMFs are nearly orthogonal to each other, we have the total energy for the data  $f_j$  for  $j = 1, 2, \dots, N$ , to a high degree of approximation, as

$$\sum_{j=1}^N f_j^2 = \sum_{k=1}^N |F_k|^2 = N \sum_n E_n. \quad (5.3)$$

In (5.3),

$$F_k = \sum_{j=1}^N f_j e^{-2\pi i j k / N} \quad (5.4)$$

is the Fourier transform of data  $f_j$ , and

$$E_n = \frac{1}{N} \sum_{j=1}^N [C_n(j)]^2 \quad (5.5)$$

is the energy density of the  $n$ th IMF, where  $i = \sqrt{-1}$ ,  $|F_k|$  is the norm of  $F_k$ , and  $C_n(j)$  is the  $n$ th IMF. The expected Fourier spectrum of a white noise time series is a constant, indicating that the contribution to the total spectrum energy comes from each Fourier component uniformly and equally. (For a synthetically generated white noise time series of short length, however, its Fourier spectrum may be a constant superimposed on by many spikes. The spikes of the Fourier spectrum of an individual copy will be smoothed out when the Fourier spectra of many copies of white noise series of the same length are averaged, and the average of the Fourier spectra approaches a constant.) The Fourier spectra for the IMFs, however, will not

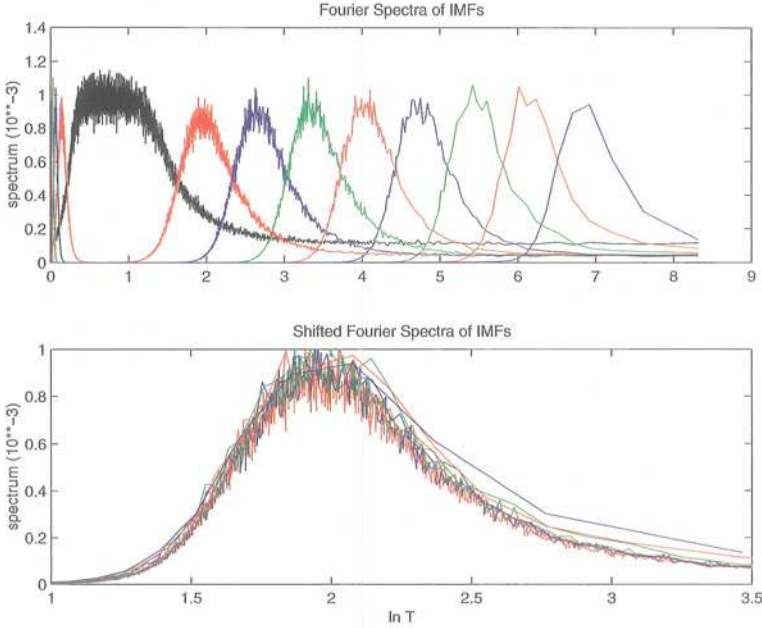


**Figure 5.1:** The Fourier spectra of IMFs as a function of the logarithm of their periods. In the upper panel, the black line is the Fourier spectrum of the first IMF, and the Fourier spectra of IMFs 2-9 are located away from that of the first IMF, respectively. In the lower panel, the Fourier spectra of IMFs 2-9 are redrawn and the Fourier spectrum of the  $n$ th IMF is shifted to the left by  $(n - 2) \ln(2)$  for IMFs 3-9.

yield a constant white spectrum, for the decomposition through EMD effectively subjects the data to a dyadic filter (Flandrin et al. 2004).

To illustrate the shape of the Fourier spectrum for each IMF, the Fourier spectra of 256 ( $2^8$ ) independent segments of 4096 ( $2^{12}$ ) data points each are calculated. The averaged Fourier spectra for nine IMFs are plotted on a semi-logarithmic scale in Fig. 5.1. It is clear that all the Fourier spectra, except the first one, have almost identical shapes in terms of the  $\ln(T)$ -axis, where  $T$  is the period of a Fourier component. Figure 5.1 implies that the ratios of the periods of the neighboring spectra are almost identically equal to 2, a fact consistent with the doubling of the mean periods of the neighboring IMFs.

Based on the fact of identical spectral shape and identical area coverage for each IMF, an approximate integral expression of the functional form of the Fourier spectrum for any IMF, except the first one, can be made as

$$\int S_{\ln(T),n} d[\ln(T)] = \text{constant}, \quad (5.6)$$

where  $S_{\ln(T),n}$  denotes the Fourier spectrum of the  $n$ th IMF as a function of  $\ln(T)$ , and the subscript  $n$  denotes the  $n$ th IMF. From (5.6), one can derive for a normalized

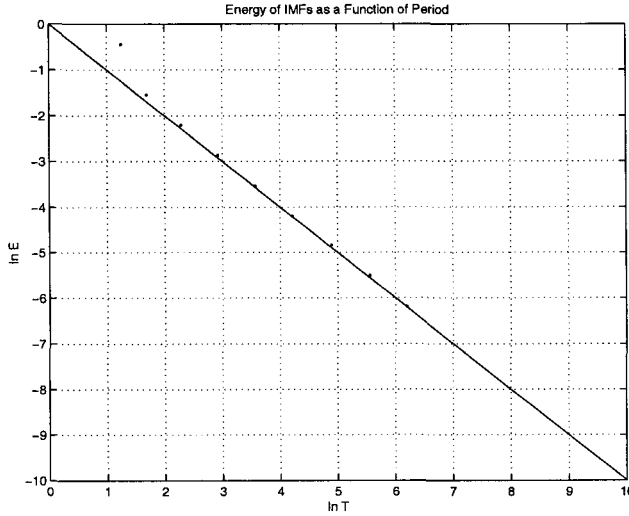


**Figure 5.2:** The relation between the energy density and the spectrum-weighted mean period. The black dots are the energy density as a function of the spectrum-weighted mean period for IMFs 1–9 based on the Fourier spectra displayed in Fig. 5.1. The black straight line from upper left to lower right is the theoretical line corresponding to (5.7).

Gaussian white noise series that

$$\ln(\bar{E}_n) + \ln(\bar{T}_n) = 0, \quad (5.7)$$

where

$$\bar{T}_n = \frac{\int S_{\ln(T),n} d[\ln(T)]}{\int S_{\ln(T),n} d[\ln(T)]/T} \quad (5.8)$$

is the spectrum-weighted mean period of  $n$ th IMF as  $N \rightarrow \infty$ . The simple relation in (5.7) has already been stated in Wu et al. (2001).

The verification of (5.9) is given in Fig. 5.2, where the spectrum-weighted mean periods for IMFs 1-9 are calculated based on the averaged Fourier spectra of the corresponding IMFs displayed in Fig. 5.1. The straight black line from the upper left to the lower right is the expectation line derived from (5.9). Clearly, (5.9) offers an excellent fit to these scattered points.

#### 5.2.4. Probability distributions of IMFs and their energy

In this subsection, we will examine the probability density functions of IMFs and their corresponding energy. Before we present the results, we re-examine the mathematical meanings of IMFs. To achieve this goal, we rewrite part of (5.3) as

$$f_j = \sum_{i=1}^n C_i(j) = \sum_{i=1}^m C_i(j) + R_m(j) = \sum_{i=1}^{m+1} C_i(j) + R_{m+1}(j), \quad (5.9)$$

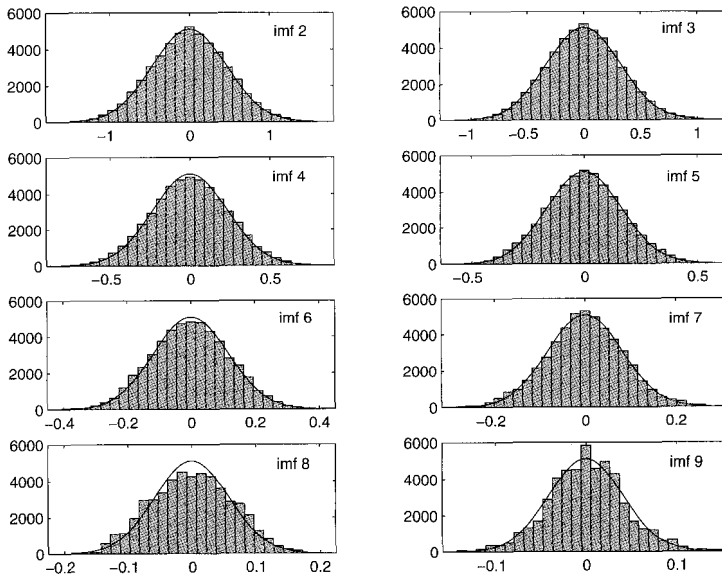
where  $R_m(j)$  is the remainder of  $f_j$  after  $m$  number of IMFs are extracted. It is easy to recognize that

$$R_i(j) = C_{i+1}(j) + R_{i+1}(j). \quad (5.10)$$

Since  $C_{i+1}(j)$  is purely oscillatory with respect to  $R_{i+1}(j)$ , we can consider  $R_{i+1}(j)$  as the local mean of  $R_i(j)$ . Similarly,  $R_i(j)$  is the local mean of  $R_{i-1}(j)$  and so forth, so that  $R_2(j)$  is the local mean of  $R_1(j)$ . Therefore,  $R_{i+1}(j)$  can also be considered as the local mean of  $f_j$  over a local timescale that is approximately the local period of  $C_{i+1}(j)$ . Since the local period of  $C_{i+1}(j)$  is concentrated near the extrema-counting mean period of  $C_{i+1}(j)$ , to a good approximation, the distribution of  $R_{i+1}(j)$  is close to the distribution of the running mean of  $f_j$  over the extrema-counting mean period of  $R_i(j)$ .

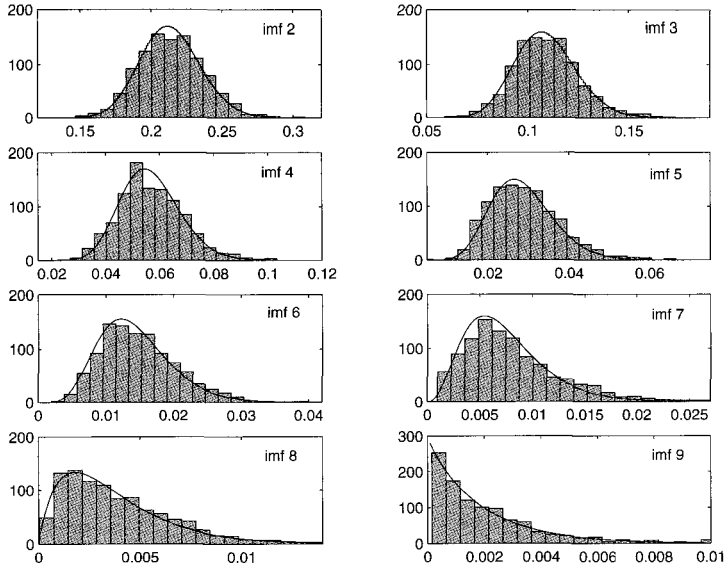
Two major theorems in statistics (Papoulis, 1986) can then be applied to infer the distribution of  $C_{i+1}(j)$ . The first one is the central limit theorem, which states that the mean over a given finite number of random samples from a distribution with finite variance results in a normal distribution. Therefore,  $R_i(j)$  and  $R_{i+1}(j)$  are both approximately normal distributions. The second theorem states that the linear combination of two normal distributions results in another normal distribution. Therefore, we can infer that all IMFs of Gaussian white noise are approximately normally distributed.

Figure 5.3 plots the probability distribution of each IMF for a sample of 50 000 data points. The results are consistent with the discussion we presented above.



**Figure 5.3:** The histograms of IMFs (modes) 2–9 for a white noise sample with 50 000 data points. The superimposed black lines are the Gaussian fitting for each IMF.





**Figure 5.4:** The histograms of the energy density for IMFs (modes) 2–9 for 1024 white noises samples of 1024 data points each. The superimposed black lines are the chi-square fitting for each IMF.

Indeed, the deviation from the normal distribution function grows as the mode number increases because in the higher modes, the IMFs contain a small number of oscillations; therefore, the number of events decrease, and the distribution becomes less smooth. When a sample of longer length is used, the IMFs of the higher modes will have more oscillations, and the distribution will converge to a normal distribution according to the central limit theorem.

According to the theory of probability density function, for a time series that has a normal distribution, its energy defined by (5.5) should have a *chi-square* distribution with the degrees of freedom of the chi-square distribution equal to the mean of the energy.

To determine the exact number of degrees of freedom for the chi-square distribution of IMFs decomposed from a white noise series of length  $N$ , we can argue as follows: we use the Fourier spectrum of a white noise series of the same length,  $N$ . For such a white noise series, its number of degrees of freedom is  $N$ , and that number is an invariant when the data are mapped into another space. The decomposition of such a white noise series in terms of Fourier components results in  $N$  Fourier components which form a complete set. Each component has a unit degree of freedom; therefore, the number of degrees of freedom of an IMF is essentially the sum of the Fourier components it contains. As the energy in a white noise series is evenly distributed to each Fourier components, we propose that the fraction of energy contained in an IMF is the same as the fraction of the number of degrees of freedom. For a normalized white noise time series with unit total energy, the number

of degrees of freedom of the  $n$ th IMF should be the energy of that particular IMF; thus,  $r_n = N\bar{E}_n$ . Therefore, the probability distribution of  $NE_n$  is the chi-square distribution with  $N\bar{E}_n$  degrees of freedom:

$$\rho_N(NE_n) = (NE_n)^{N\bar{E}_n/2-1} e^{-NE_n/2}. \quad (5.11)$$

Therefore, the probability distribution of  $E_n$  is

$$\rho(E_n) = N(NE_n)^{N\bar{E}_n/2-1} e^{-NE_n/2}. \quad (5.12)$$

A Monte Carlo test confirms our conjecture. Figure 5.4 shows the histogram of the distribution of energy for each IMF for 1024 samples of white noise series each of the length of 1024 data points. The red lines are the corresponding chi-square distributions based on (5.12). Clearly, the theoretical lines and histograms are in excellent agreement with each other.

### 5.3. Spread functions of mean energy density

Having determined the distribution function of the energy, we are ready to derive the spread of the energy densities of the IMFs of white noise samples of certain length  $N$ . Since the characteristics of Gaussian white noise are essentially identical to those of the uniformly distributed white noise that we described in Wu and Huang (2003, 2004), the spreads of the energy density of the IMFs of Gaussian white noise are also the same as the results we obtained in Wu and Huang (2003, 2004). Here, we repeat the derivation of functions that we included in Wu and Huang (2003, 2004).

Since the probability distribution of energy density  $E_n$  is given by (5.12), we can derive the probability distribution of a new variable  $y = \ln(E)$  as

$$\begin{aligned} \rho(y) &= N(Ne^y)^{N\bar{E}/2-1} e^{-NE/2} e^y \\ &= C \exp\left(y \frac{N\bar{E}}{2} - \frac{NE}{2}\right) = C \exp\left[-\frac{N\bar{E}}{2} \left(\frac{E}{\bar{E}} - y\right)\right], \end{aligned} \quad (5.13)$$

where  $C = N^{N\bar{E}/2}$ . For simplicity, the subscript  $n$  is omitted in (5.13). Since

$$\frac{E}{\bar{E}} = e^{y-\bar{y}} = 1 + y - \bar{y} + \frac{(y-\bar{y})^2}{2!} + \frac{(y-\bar{y})^3}{3!} + \dots, \quad (5.14)$$

substituting (5.14) into (5.13) leads to

$$\begin{aligned} \rho(y) &= C \exp\left\{-\frac{N\bar{E}}{2} \left[1 - \bar{y} + \frac{(y-\bar{y})^2}{2!} + \frac{(y-\bar{y})^3}{3!} + \dots\right]\right\} \\ &= C' \exp\left\{-\frac{N\bar{E}}{2} \left[\frac{(y-\bar{y})^2}{2!} + \frac{(y-\bar{y})^3}{3!} + \dots\right]\right\}, \end{aligned} \quad (5.15)$$

where  $C' = C \exp[-N\bar{E}(1-\bar{y})/2]$ . From (5.15), one can determine the spread of the different confidence levels.

When  $|y - \bar{y}| \ll 1$ ,

$$\rho(y) = C \exp \left\{ -\frac{N\bar{E}}{2} \left[ 1 - \bar{y} + \frac{(y - \bar{y})^2}{2!} \right] \right\} = C' \exp \left[ -\frac{N\bar{E}(y - \bar{y})^2}{4} \right], \quad (5.16)$$

Therefore, the distribution of  $y = \ln(E)$  is approximately a Gaussian with a standard deviation of

$$\sigma^2 = \frac{2}{N\bar{E}} = \frac{2\bar{T}}{N}. \quad (5.17)$$

For such a case, the spread lines can be approximately defined as

$$y = -x \pm k \sqrt{\frac{2}{N}} e^{x/2}, \quad (5.18)$$

where  $x = \ln(\bar{T}_n)$  and  $k$  is a constant determined by percentiles of a standard normal distribution. For example, when  $k = -2.326, -0.675, 0.0, 0.675$ , and  $2.326$ , we obtain the first, 25th, 50th, 75th and 99th percentiles, respectively.

Figure 5.5 plots the spread lines for the 5th and 95th percentiles based on (5.15)–(5.16), as well as the scattered pairs of the mean energy density and spectrum–

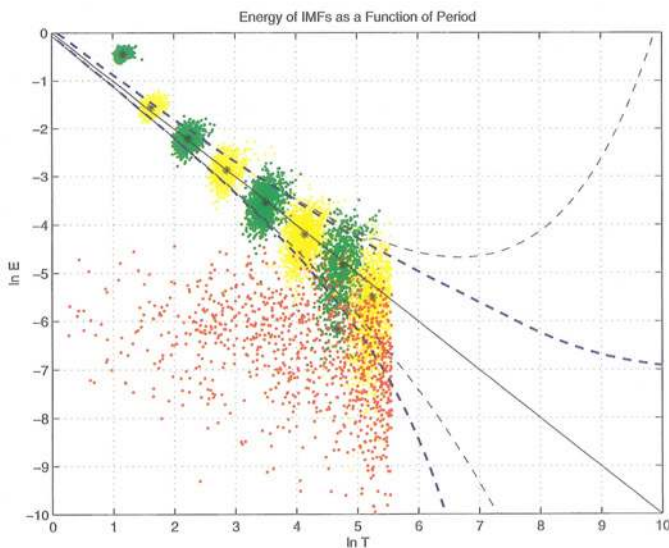


**Figure 5.5:** The spread function. The grouped green and yellow dots from the upper left to the lower right are the mean energy density as a function of the spectrum-weighted mean period for IMFs 1–8 for all 1024 samples with an identical length of 1024 data points. The grouped red dots are the same as the green and yellow dots except they are for IMF 9. The solid black line from the upper-left corner to the lower-right corner is the same as in Fig. 5.2. The bold dashed lines are the first and 95th percentiles calculated from (5.15). The thin dashed lines are the first and 95th percentiles calculated from (5.16). The asterisks correspond to the pairs of the averaged mean energy density and the averaged spectrum-weighted mean period of all 1024 samples for each IMF.

weighted mean period for the IMFs of each sample of 1024 data points. In this figure, the Fourier spectra of the IMFs of each sample are obtained through the Fourier transform of the IMFs of 1024 data points, which is a quarter of the length of the samples used to calculate the Fourier spectra in Fig. 5.2.

In general, the Monte Carlo results displayed in Fig. 5.5 agree well with the theoretical inferences discussed above. The simplified calculations based on (5.18) agree well with the theoretical lines (bold dashed) that are based on (5.16), which provide more details of the abnormal distribution that skews toward the lower energy side. However, for slowly oscillating IMFs, the averages of the spectrum-weighted mean period deviate from the theoretical line (the bold black) significantly. For example, the scattered pairs of the mean energy density and the spectrum weighted mean period (red dots) for IMF 9, as well as their averages, are located systematically on the lower-left side of the theoretical expectation line of the mean energy density and the spectrum weighted mean period. As is evident in Fig. 5.2, such a large systemic error is not seen when the spectra are calculated by using longer samples, because the Fourier transform of a short piece of a slowly oscillating IMF with a large mean period is likely to represent artificially the low frequency components of the IMF with high-frequency components. Such drawbacks of the Fourier transform do not affect the high-frequency IMFs much since these IMFs do not contain much low-frequency information, but can lead to the severe overestimation (underestimation) of the mean frequency (spectrum-weighted mean period) of slowly oscillating IMFs.

The problem mentioned above has negative implications for designing a statistical significance test method for IMFs based on the characteristics of Gaussian white noise that we discussed previously: the spread lines of a certain percentage work only for IMFs of high frequency but not for IMFs of low frequency. To eliminate the problem, we need to search for a better estimation of the mean periods of IMFs. Fortunately, the extrema-counting and Hilbert transform lead to quite an accurate estimation of the mean period. The methods were adopted in Wu and Huang (2003, 2004). However, the latter approach also has a side effect: the expectation line of the mean period and the energy density is likely to deviate from the theoretical line.

Figure 5.6 shows the results of the latter approach. The dashed black line is the fitting of the averaged mean energy density and the averaged mean period based on extrema counting and the Hilbert transform of all 1024 samples. This fitting can be expressed as

$$\ln(\bar{E}) = 0.12 - 0.934 \ln(\bar{T}). \quad (5.19)$$

With this empirical correction and the spread function of energy density expressed by (5.15), we can obtain the lines for the various confidence levels. for the 5th and 95th percentiles are shown by the bold dashed lines. Clearly, these lines are consistent with the Monte Carlo test.

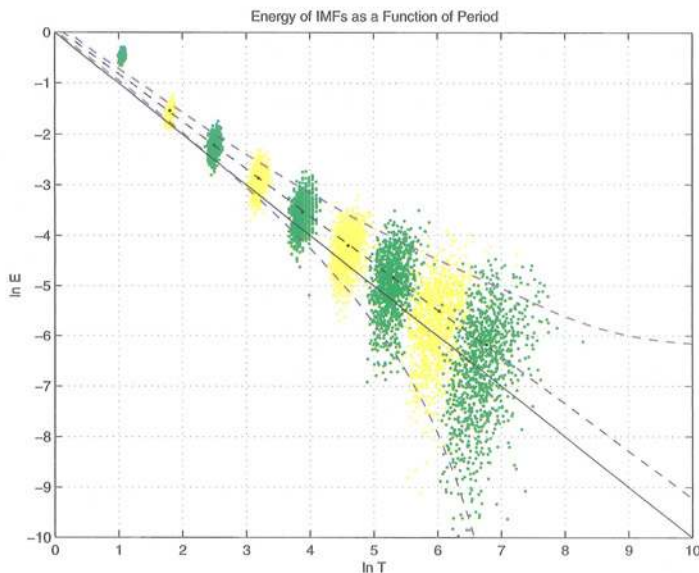


**Figure 5.6:** Same as Fig. 5.5 except that the abscissa is now the spectrum-weighted mean period for IMFs 1-9. There are no red dots or asterisks. The black dots correspond to the pairs of averaged mean energy density and averaged extrema-counting mean period.

#### 5.4. Examples of a statistical significance test of noisy data

The relationship between the energy density and the average period, the energy distribution, and its spread function for Gaussian white noise (which is confirmed by Monte Carlo tests) revealed in previous sections provides a unique opportunity for us to design a method to distinguish IMFs of a dataset from those of pure Gaussian white noise, so that we can determine which IMFs from a dataset contain information, and which IMFs may be only components of the pure Gaussian white noise that is contained in this dataset. The method is based on the rejection of a null hypothesis, which states that all IMFs are the components of a pure Gaussian white noise dataset. Our goal is to demonstrate that the null hypothesis is an untrue statement about the origin of these IMFs. If the possibility is small (say, less than 0.05) that the IMFs decomposed from the noisy dataset could be the results of the decomposition of any Gaussian white noise of the same length as that of the targeted dataset, we reject the null hypothesis and consider that these IMFs contain signal information. With this consideration in mind, we design a significance test method utilizing the statistical characteristics of Gaussian white noise, which, by definition, contains no information. The method is then simple: first, decompose the targeted noisy dataset (normalized) into IMFs; second, use (5.15) to calculate the spread function of given percentiles for the IMFs decomposed from Gaussian white noise; third, select the confidence-limit level (e.g., 95%) and determine the upper and lower spread lines; and finally, compare the energy density for the IMFs from

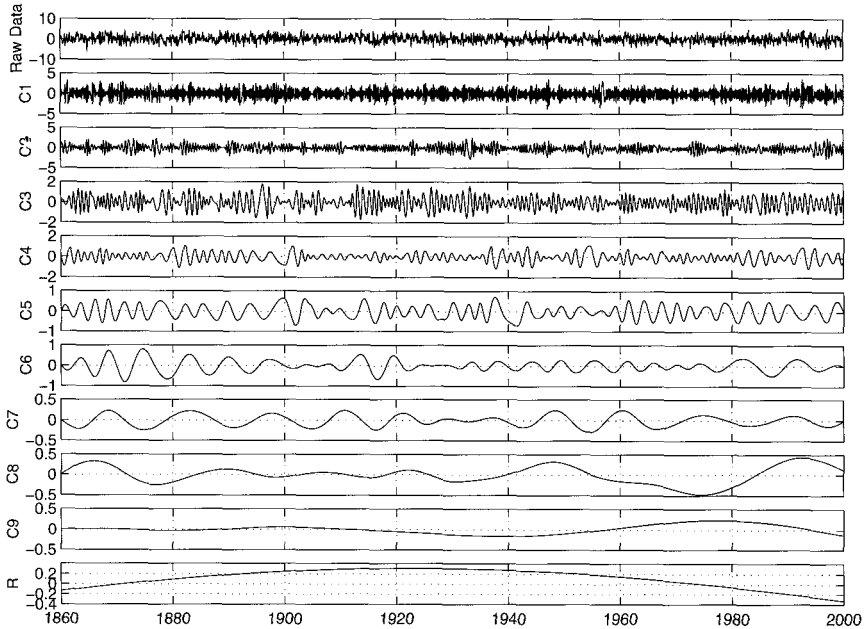


**Figure 5.7:** The raw NAOI (top panel), the corresponding intrinsic mode functions ( $C1 - C9$ ), and the trend ( $R$ ).

the noisy data with the spread functions. The IMFs with their energy located above the upper bound or below the lower bound should be considered as containing signal information at that selected confidence level. In the final step, if the targeted dataset is non-stationary and has a large trend, the trend should be excluded, and all the oscillatory IMFs should be rescaled by using the total energy of all the oscillatory IMFs.

In the following, we will use EMD to decompose three well-known time series in climate study: (1) the North Atlantic Oscillation Index (NAOI, monthly data from January 1860 to December 1999); (2) the Southern Oscillation Index (SOI, monthly data from January 1866 to December 1997); and (3) the globally averaged surface temperature anomaly (GASTA, monthly data from January 1860 to December 1999). The decompositions of these indices use the same sifting stoppage criterion as that used in (5.2). The indices being analyzed here are all maintained by P. Jones of the Climate Research Unit, University of East Anglia. The advantages and drawbacks of our proposed significance testing method will be illustrated when the method is applied to test the IMFs of these three time series.

#### 5.4.1. Testing of the IMFs of the NAOI

The North Atlantic Oscillation (NAO) is a well-known climate pattern that has great impact on Europe's climate. The NAO is often indexed by the difference

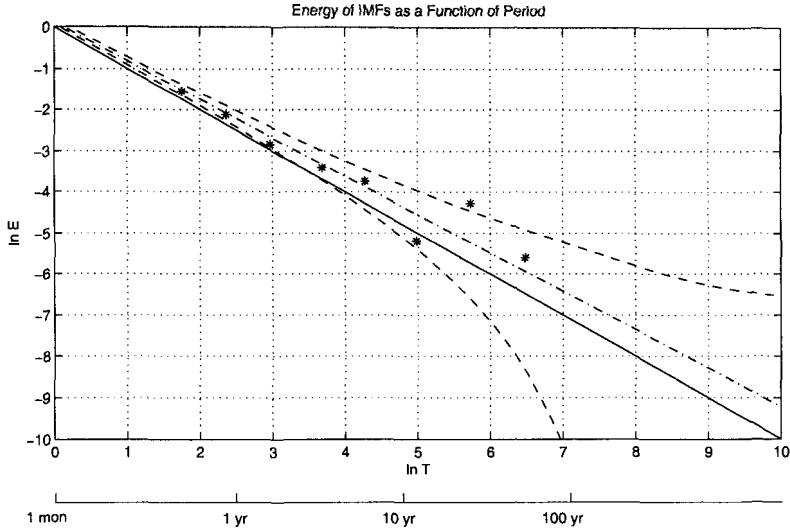


**Figure 5.8:** Significance test of the IMFs of the NAOI. The solid line from the upper-left corner to the lower-right corner is the same as in Fig. 5.6. The dash-dotted black line is the empirical fitting of the averaged mean energy density and the averaged mean period for Gaussian white noise. The dashed lines are the 5th and 95th percentiles calculated from (5.16). The asterisks correspond to the pairs of the averaged mean energy density and the averaged mean period of  $C2 - C9$  of NAOI (from left to right).

in sea-level pressure between Iceland, representing the strength of the Icelandic climatological low, and the Azores of Lisbon (NAOI), near the central ridge of the Azores high. When the index is high, the Icelandic low is strong. This result increases the influence of the cold Arctic air masses on the northern seaboard of North America and enhances the ability of the eastward winds to carry warmer, moister air masses into western Europe during winter (Hurrell 1995). Thus, NAO anomalies are related to the downstream wintertime temperature and precipitation across Europe, Russia, and Siberia.

The NAOI being analyzed in this paper is described in Hurrell (1995) and Jones et al. (1997). As is well known among climatologists, the NAOI is a Gaussian-white-noise-like index. The auto-correlation of the NAOI with one data point lag is 0.088. Therefore, we expect that our method will generally show that most of the IMFs of the NAOI should be located between the 5% and 95% confidence levels.

The result of the testing is presented in Fig. 5.8. IMFs 2–7 and 9 are not distinguishable from the IMFs of the Gaussian white noise at the 95% confidence level. IMF 8 seems to be statistically significant at the 95% level. However, it cannot survive when the significance level is raised to 99%. The apparent significance of IMF 8 is not very surprising, since the NAOI does have a small auto-correlation. Overall, the application of our proposed testing method on a Gaussian-white-noise-like dataset is successful.

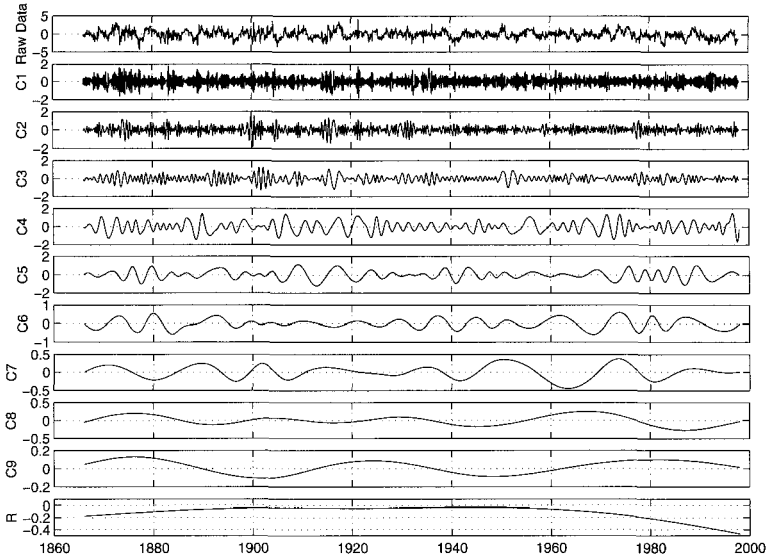


Figure 5.9: Same as Fig. 5.7, but for SOI.

#### 5.4.2. Testing of the IMFs of the SOI

The Southern Oscillation Index (SOI) is a normalized monthly sea level pressure index that reflects primarily the large-scale dynamically coupled system of atmosphere and ocean in the tropical Pacific (Trenberth 1984). A large negative (positive) peak of SOI, which often happens at two-to-seven-year intervals, corresponds to a strong El Niño (La Niña) event. With its rich statistical properties and scientific importance, the SOI is one of the most prominent time series in the geophysical research community and has been well studied. Many time-series-analysis tools have been used to analyze this time series to display their ability to reveal useful scientific information (e.g., Wu et al. 2001; Ghil et al. 2002).

The SOI that we use in this study is described in Ropelewski and Jones (1987) and Allan et al. (1991). The SOI has a lag-one auto-correlation of 0.69, indicating that it is significantly different from Gaussian white noise. The SOI and its IMFs are displayed in Fig. 5.9. The statistical significance test of the IMFs is displayed in Fig. 5.10.

The test shows that 5 IMFs are significant at the 95% confidence level. The averaged periods for these IMFs are 2.3 yr, 4.5 yr, 8.5 yr, 16.5 yr, and 32.9 yr, respectively. However, the latter two IMFs are not statistically significant at the 99% confidence level. This test result is consistent with the statistical test using the regular spectral analysis method, which also shows that the SOI has inter-annual peaks that are statistically significant.



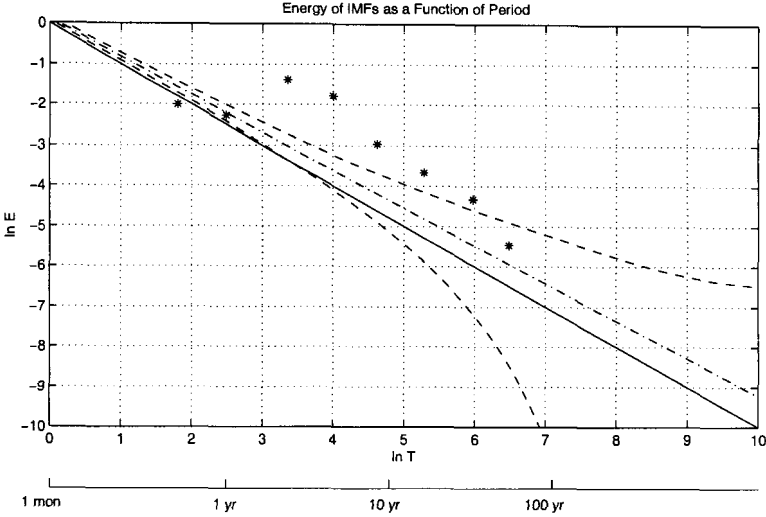


Figure 5.10: Same as Fig. 5.8, but for SOI.

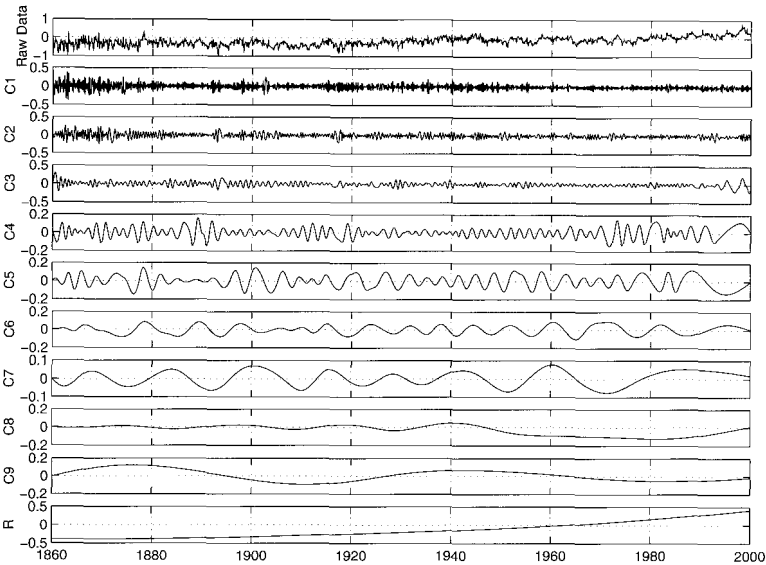


Figure 5.11: Same as Fig. 5.7, but for GASTA.

### 5.4.3. Testing of the IMFs of the GASTA

The globally averaged surface temperature anomaly (GASTA) is one of the most popular time series in the climate, environmental, and even the social sciences. It includes the responses to the strengthening anthropogenic forces such as

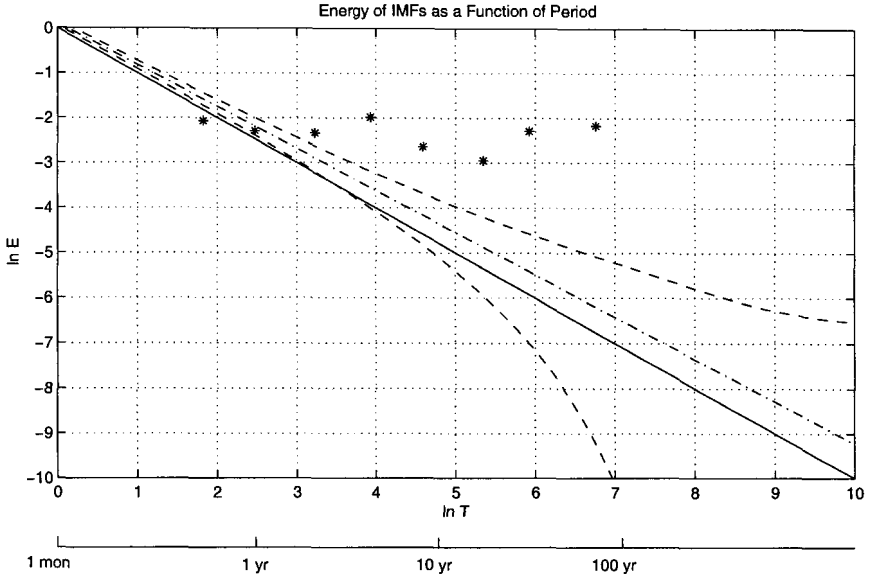


Figure 5.12: Same as Fig. 5.8, but for GASTA.

accumulating green house gases in the Earth's atmosphere and deforestation in many regions, in addition to the natural variability of the Earth's climate. Therefore, the GASTA is composed by two parts: a strong trend and oscillatory variations on all timescales. To examine whether an IMF comes from pure noise, we must first extract the trend part. Fortunately, the EMD method naturally separates the trend from the oscillatory variability in data, so we determine whether an IMF is significant at a certain confidence level after the IMF has been normalized by the total energy of all the oscillatory components.

The GASTA that we use in this study is introduced and studied in Jones et al. (1999), Folland et al. (2001a), and Folland et al. (2001b). The GASTA and its IMF components are displayed in Fig. 5.11. It is clear that the trend is very large. The temperature increased by about  $0.8^{\circ}\text{C}$  over 140 yr from 1860 to 2000.

The significance test of IMFs 2–9 is displayed in Fig. 5.11. The results reveal that IMFs 4–9 are significant. However, this conclusion is misleading. In the discussions that we presented so far in this chapter, we have implicitly or explicitly assumed that the noise included in data has been Gaussian white noise. However, the possibility cannot be ruled out that the noise in the data is not Gaussian white noise. If the GASTA does not contain Gaussian white noise, the statistical significance of an IMF against Gaussian white noise does not mean the IMF is physically or even statistically significant. Indeed, the oscillatory part of GASTA is more like a fractional Gaussian noise (fGn) series with its Hurst exponent close to 0.9. Therefore, we must be cautious about concluding that an IMF is statistically significant.

#### 5.4.4. *A posteriori* test

The examples presented above are all *a priori* tests in which we do not know the noise level in the data. However, if we can ascertain that any specific IMF contains little useful information, then we can assume that the energy of that IMF comes solely from noise, and assign it on the 99% line. Then, we can use the energy level of that IMF to re-scale the rest of the IMFs. If the energy level of any IMF lies above the theoretical reference white noise line, we can assume that this IMF contains statistically significant information. If the rescaled energy level lies below the theoretical white noise line, then we can assume that the IMF contains little useful information. The latter is called a *posteriori* test. An example of a *posteriori* test is included in Wu and Huang (2003, 2004).

#### 5.5. Summary and discussion

The properties of Gaussian white noise were studied by using the EMD method. We carried out numerical experiments to decompose uniformly distributed white noise into IMFs. The empirical findings were almost identical to those given in Wu and Huang (2003, 2004) for uniformly distributed white noise. Therefore, we followed the example of Wu and Huang (2003, 2004) when we deduced expressions for the various statistical properties of Gaussian white noise. These results were all tested by using the Monte Carlo method.

The known characteristics of Gaussian white noise were used to design statistical test methods that were applied to three well-known climate time series: (1) the North Atlantic Oscillation index (NAOI), which is close to pure Gaussian white noise; (2) the Southern Oscillation index (SOI), which contains dominant oscillation on interannual timescales; and (3) the global averaged surface temperature anomaly (GASTA), which contains a large trend and possibly noise other than Gaussian white noise. The tests of the NAOI and the SOI obtained results consistent with those of the tests using Fourier analysis methods, indicating that our methods are valid and effective when data contain Gaussian white noise. The results of the test of the GASTA, which likely contains other types of noise, seem to exaggerate the significance of some IMFs. To eliminate this problem, the methods that can test against other types of noise should be used. Our proposed testing method is not just a trivial testing method, but is consistent with other analysis methods. The EMD method's results give us the following additional information: First, EMD identifies the significant IMFs. Because IMFs are adaptive, they can represent the underlying processes more effectively than pure sinusoids. Furthermore, the IMFs isolate physical processes of various time scales and also give the temporal variation with the processes in their entirety without resorting to the linear assumption as in the Fourier-based decomposition. Because we are free of harmonics, the IMFs can show the nonlinear distortion of the waveform locally, as was discussed by Huang et al. (1998) and Wu et al. (2001). Finally, the IMFs can be used to construct the

time-frequency distribution in the form of the Hilbert spectrum, which offers minute details of the time variation of the underlying processes.

A *posteriori* test method was also discussed. The IMFs are more effective in isolating the physical processes of various timescales than the usual Fourier component.

### Acknowledgements

The authors would like to thank Professor Samuel Shen of the University of Alberta for suggesting to us to study the Fourier spectra of the IMFs from the white noise. Throughout our study, he also offered valuable comments and encouragement. The authors also gratefully acknowledge the assistance of Dr. Dean G. Duffy at NASA/GSFC in preparing our manuscript. ZW is supported by NSF under grant ATM-0342104, and NEH is supported in part through a grant from NASA RTOP Oceanic Processes Program, an ONR Processes and Prediction Program grant number N00014-98-F-0412, and a NOAA Climate Center grant number NEEF4100-3-00269.

### References

- Allan, R. J., N. Nicholls, P. D. Jones, and I. J. Butterworth, 1991: A further extension of the Tahiti-Darwin SOI, early ENSO events and Darwin pressure. *J. Climate*, **4**, 743–749.
- Flandrin, P., G. Rilling, and P. Gonçalvès, 2004: Empirical mode decomposition as a filter bank. *IEEE Signal Process. Lett.*, **11**, 112–114.
- Folland, C. K., N. A. Rayner, S. J. Brown, T. M. Smith, S. S. P. Shen, D. E. Parker, I. Macadam, P. D. Jones, R. N. Jones, N. Nicholls, and D. M. H. Sexton, 2001a: Global temperature change and its uncertainties since 1861. *Geophys. Res. Lett.*, **28**, 2621–2624.
- Folland, C. K., T. R. Karl, J. R. Christy, R. A. Clarke, G. V. Gruza, J. Jouzel, M. E. Mann, J. Oerlemans, M. J. Salinger, and S.-W. Wang, 2001b: Observed climate variability and change. *Climate Change 2001: The Scientific Basis*, J. T. Houghton, Y. Ding, D. J. Griggs, M. Noguer, P. J. van der Linden, X. Dai, K. Maskell, and C. A. Johnson, Eds., Cambridge University Press, 99–181.
- Ghil, M., M. R. Allen, M. D. Dettinger, K. Ide, D. Kondrashov, M. E. Mann, A. W. Robertson, A. Saunders, Y. Tian, F. Varadi, and P. Yiou, 2002: Advanced spectral methods for climatic time series. *Rev. Geophys.*, **40**, 10.1029/2000GR000092.
- Huang, N. E., Z. Shen, S. R. Long, M. C. Wu, H. H. Shih, Q. Zheng, N.-C. Yen, C. C. Tung, and H. H. Liu, 1998: The empirical mode decomposition and the Hilbert spectrum for nonlinear and non-stationary time series analysis. *Proc. R. Soc. London, Ser. A*, **454**, 903–995.
- Huang, N. E., Z. Shen, and S. R. Long, 1999: A new view of water waves – The Hilbert spectrum. *Annu. Rev. Fluid Mech.*, **31**, 417–457.

- Hurrell, J.W., 1995: Decadal trends in the North Atlantic Oscillation and relationships to regional temperature and precipitation. *Science*, **269**, 676–679.
- Jones, P. D., T. Jonsson, and D. Wheeler, 1997: Extension using early instrumental pressure observations from Gibraltar and SW Iceland to the North Atlantic Oscillation. *Int. J. Climatol.*, **17**, 1433–1450.
- Jones, P. D., M. New, D. E. Parker, S. Martin, and I. G. Rigor, 1999: Surface air temperature and its variations over the last 150 years. *Rev. Geophys.*, **37**, 173–199.
- Papoulis, A., 1986: *Probability, Random Variables, and Stochastic Processes*. McGraw-Hill, 576 pp.
- Press, W. H., S. A. Teukolsky, W. T. Vetterling, and B. P. Flannery, 1992: *Numerical Recipes in C*. Cambridge University Press, 994 pp.
- Ropelewski, C. F., and P. D. Jones, 1987: An extension of the Tahiti-Darwin Southern Oscillation Index. *Mon. Wea. Rev.*, **115**, 2161–2165.
- Trenberth, K. E., 1984: Signal versus noise in the Southern Oscillation. *Mon. Wea. Rev.*, **112**, 326–332.
- Wu, Z., E. K. Schneider, Z.-Z. Hu, and L. Cao, 2001: The impact of global warming on ENSO variability in climate records. *COLA Technical Rep. 110*, 24 pp.
- Wu, Z., and N. E. Huang, 2003: A study of the characteristics of white noise using the empirical mode decomposition method. *COLA Technical Rep. 133*, 27 pp.
- Wu, Z., and N. E. Huang, 2004: A study of the characteristics of white noise using the empirical mode decomposition method. *Proc. R. Soc. London, Ser. A*, **460**, 1597–1611.

Zhaohua Wu

Center for Ocean-Land-Atmosphere Studies, 4041 Powder Mill Road, Suite 302,  
Calverton, MD 20705, USA

zhwu@cola.iges.org

Norden E. Huang

Goddard Institute for Data Analysis, Code 614.2, NASA/Goddard Space Flight  
Center, Greenbelt, MD 20771, USA

norden.e.huang@nasa.gov